Specific collagen XVIII isoforms promote adipose tissue accrual via mechanisms determining adipocyte number and affect fat deposition

Mari Aikio[a,b,1], Harri Elamaa[a,b,1], David Vicente[a,b], Valerio Izzi[a,b], Inderjeet Kaur[a,b], Lotta Seppinen[a,b], Helen E. Speedy[c], Dorota Kaminska[d], Sanna Kuusisto[b,e], Raija Sormunen[b,f], Ritva Heljasvaara[a,b], Emma L. Jones[c], Mikko Muilu[g], Matti Jauhiainen[g], Jussi Pihlajamäki[d,h], Markku J. Savolainen[b,e], Carol C. Shoulders[c,2], and Taina Pihlajaniemi[a,b,2]

[a]Faculty of Biochemistry and Molecular Medicine, Oulu Center for Cell-Matrix Research, [b]Biocenter Oulu, [e]Department of Internal Medicine, Clinical Research Center, Institute of Clinical Medicine, and [f]Department of Pathology, Oulu University Hospital, University of Oulu, FI-90014 Oulu, Finland; [c]Centre for Endocrinology, William Harvey Research Institute, Queen Mary University of London and Barts and the London School of Medicine and Dentistry, London EC1M 6BQ, United Kingdom; [d]Department of Clinical Nutrition, Institute of Public Health and Clinical Nutrition, University of Eastern Finland, FI-70211 Kuopio, Finland; [g]Public Health Genomics Unit, National Institute for Health and Welfare, FI-00290 Helsinki, Finland; and [h]Department of Medicine, Clinical Nutrition and Obesity Center, Kuopio University Hospital, FI-70211 Kuopio, Finland

Edited* by Darwin J. Prockop, Texas A&M Health Science Center, Temple, TX, and approved June 16, 2014 (received for review April 1, 2014)

Collagen XVIII is an evolutionary conserved ubiquitously expressed basement membrane proteoglycan produced in three isoforms via two promoters (*P*). Here, we assess the function of the N-terminal, domain of unknown function/frizzled-like sequences unique to medium/long collagen XVIII by creating *P*-specific null mice. *P2*-null mice, which only produce short collagen XVIII, developed reduced bulk-adiposity, hepatic steatosis, and hypertriglyceridemia. These abnormalities did not develop in *P1*-null mice, which produce medium/long collagen XVIII. White adipose tissue samples from *P2*-null mice contain larger reserves of a cell population enriched in early adipocyte progenitors; however, their embryonic fibroblasts had ∼50% lower adipocyte differentiation potential. Differentiating 3T3-L1 fibroblasts into mature adipocytes produced striking increases in *P2* gene-products and dramatic falls in *P1*-transcribed mRNA, whereas Wnt3a-induced dedifferentiation of mature adipocytes produced reciprocal changes in *P1* and *P2* transcript levels. *P2*-derived gene-products containing frizzled-like sequences bound the potent adipogenic inhibitor, Wnt10b, in vitro. Previously, we have shown that these same sequences bind Wnt3a, inhibiting Wnt3a-mediated signaling. *P2*-transcript levels in visceral fat were positively correlated with serum free fatty acid levels, suggesting that collagen α1 (XVIII) expression contributes to regulation of adipose tissue metabolism in visceral obesity. Medium/long collagen XVIII is deposited in the Space of Disse, and interaction between hepatic apolipoprotein E and this proteoglycan is lost in *P2*-null mice. These results describe a previously unidentified extracellular matrix-directed mechanism contributing to the control of the multistep adipogenic program that determines the number of precursors committing to adipocyte differentiation, the maintenance of the differentiated state, and the physiological consequences of its impairment on ectopic fat deposition.

Collagen XVIII, one of the multiplexin subfamily of nonfibrillar collagens (1), is a component of basement membranes (BM) of both epithelial and endothelial cells. Collagen XVIII has attracted much interest on several accounts. It has the structural properties of both a collagen and a proteoglycan (2); it contains the antiangiogenic molecule, endostatin (3), and its coding gene, collagen α1 (XVIII) (*COL18A1*), is mutated in the rare, recessively inherited Knobloch syndrome (4). This condition is characterized by high myopia and vitro-retinal degeneration, and occasionally by occipital encephalocele (5, 6). Epilepsy, renal anomalies, lung hypoplasia, and acute lymphoblastic leukemia also figure in isolated cases (5, 7) but it remains to be established which, if any, of these diverse features result from disturbances of collagen XVIII-mediated BM functions, the antiangiogenic actions of endostatin, or hitherto unsuspected biological activities of this proteoglycan.

Col18a1$^{-/-}$ mice recapitulate the human eye disease of Knobloch syndrome, including delayed regression of the hyaloid vessels and impaired angiogenesis of retinal vessels (8, 9). Moreover, on a specific background, *Col18a1*$^{-/-}$ mice have increased susceptibility to hydrocephalus associated with broadening of the epithelial BM of the choroid plexuses (10). Curiously, these mice also display postprandial hyperlipidemia (11) and, on an apolipoprotein E (*ApoE*)$^{-/-}$ background, develop severe atherosclerosis because of increased plaque angiogenesis and permeability of the vasculature to lipids (12). Thus, collagen XVIII is obligatory for controlling blood vessel formation in the eye, and may also partake in BM or cell-signaling functions in extraocular tissues.

An unresolved issue concerns the physiological roles of the three distinct N-terminal, noncollagenous (NC) domains of collagen XVIII (13, 14). The "short form," which is present in most vascular and epithelial BMs and around smooth and skeletal muscle (15), derives from promoter (*P*) *1* transcripts and lacks, through exon skipping, exon 3-encoded amino acid residues.

Significance

A previously unrecognized role is described for collagen XVIII—a ubiquitous, structurally complex basement membrane proteoglycan—in supporting preadipocyte differentiation and the maintenance of this differentiated state, and hence the size and lipid-clearing/storage functions of white adipose tissue depots. Specific lack of medium and long isoforms of this nonfibrillar collagen in mice led to reduced adiposity, ectopic deposition of fat in liver, and elevated very low-density lipoprotein-triglyceride levels. The finding of a previously unidentified extracellular mechanism contributing to control of adipogenesis is expected to promote understanding of the molecular and functional bases of human hyperlipidemic syndromes associated with fatty liver.

Author contributions: M.A., H.E., D.V., V.I., I.K., L.S., H.E.S., D.K., S.K., R.S., R.H., E.L.J., M.M., M.J., J.P., M.J.S., C.C.S., and T.P. designed research; M.A., H.E., D.V., V.I., I.K., L.S., H.E.S., D.K., S.K., R.S., R.H., E.L.J., M.M., M.J., J.P., M.J.S., C.C.S., and T.P. performed research; M.A., H.E., D.V., V.I., I.K., L.S., R.H., and T.P. contributed new reagents/analytic tools; M.A., H.E., D.V., V.I., I.K., L.S., H.E.S., D.K., S.K., R.S., R.H., E.L.J., M.M., M.J., J.P., M.J.S., C.C.S., and T.P. analyzed data; and M.A., H.E., D.V., V.I., H.E.S., D.K., S.K., R.S., R.H., E.L.J., M.J., J.P., M.J.S., C.C.S., and T.P. wrote the paper.

The authors declare no conflict of interest.

*This Direct Submission article had a prearranged editor.

[1]M.A. and H.E. contributed equally to this work.

[2]To whom correspondence may be addressed. Email: taina.pihlajaniemi@oulu.fi or c.shoulders@qmul.ac.uk.

This article contains supporting information online at www.pnas.org/lookup/suppl/doi:10.1073/pnas.1405879111/-/DCSupplemental.

In contrast, the medium and long variants, abundant in liver sinusoids (15), are generated from a downstream promoter (*P2*) and alternative splicing of exon 3 (16). Medium and long collagen XVIII possess an N-terminal domain of unknown function (DUF), whereas the "long" isoform alone has a domain-sharing structural identity with the extracellular domain of frizzled (Fz) receptors (17). *P2*-derived gene-products also undergo proteolytic processing, thereby producing Fz-cysteine rich sequences that bind Wnt3a in vitro and inhibits Wnt/*B*-catenin-signaling and downstream gene expression (18).

In this study, we have further investigated the consequences of complete lack of collagen XVIII and examined the individual roles of *P1*- and *P2*-derived gene-products. Mice lacking *P2*-derived DUF/Fz sequences exhibit reduced adiposity, manifesting as a reduction in the number of precursor cells that attain a mature fat-cell phenotype, increased deposition of fat in liver, and elevated very low-density lipoprotein (VLDL)-triglyceride levels. In contrast, *P1*-null mice exhibit no such abnormalities. *P2*-derived transcript levels rose dramatically following induction of adipocyte differentiation, and fell upon Wnt3a-mediated de-differentiation of mature adipocytes. The finding of a previously unidentified mechanism contributing to the development and metabolic functions of white adipose tissue (WAT) has implications for understanding the nature and causes of hyperlipidemia associated with visceral obesity and fatty liver.

Results

Ablating Medium/Long Collagen XVIII Modulates Adiposity and Liver Weights. Fig. 1*A* provides a schematic of the collagen XVIII isoforms encoded by *P1*- and *P2*-derived *Col18a1* transcripts (Fig. 1*B*). To complement studies on *Col18a1*$^{-/-}$ mice we produced mice expressing only *P1* or *P2* transcripts, as depicted in Fig. S1. Specific inactivation of exon 1 (*P1*-null, *Col18a1*$^{P1/P1}$) and deletion of exon 3 (*P2*-null, *Col18a1*$^{P2/P2}$) were confirmed by Southern blot and PCR analysis (Fig. S1) plus real-time quantitative-PCR (RT-qPCR) of liver, epididymal (e)WAT, and kidney RNA (Fig. S2). Neither *P*-null mouse models displayed compensatory rises in *Col18a1* RNA from the nontargeted promoter (Fig. S2). *Col18a1*$^{-/-}$ mice transcribed varying amounts of RNA from both promoters (Fig. S2), potentially because of placing the inactivating cassette into a 3′ *Col18a1* exon (8).

To further validate the quality of the newly created *Col18a1* mouse lines, we immunofluorescently stained the kidney, an organ that expresses all three collagen XVIII variants (19), using two antibodies: "anti–all-18," which recognizes all three collagen XVIII species, and "anti–medium/long-18," which is reactive toward the two longer variants (Fig. 1*A*). The anti–all-18 antibody strongly stained the tubuli of *P2*-null and WT mice and produced no corresponding signal in *Col18a1*$^{P1/P1}$ mice, whereas the anti–medium/long-18 antibody stained the glomeruli of the *Col18a1*$^{P1/P1}$ and WT mice kidneys, but not those of the *Col18a1*$^{P2/P2}$ animals (Fig. S3). Neither antibody stained *Col18a1*$^{-/-}$ samples,

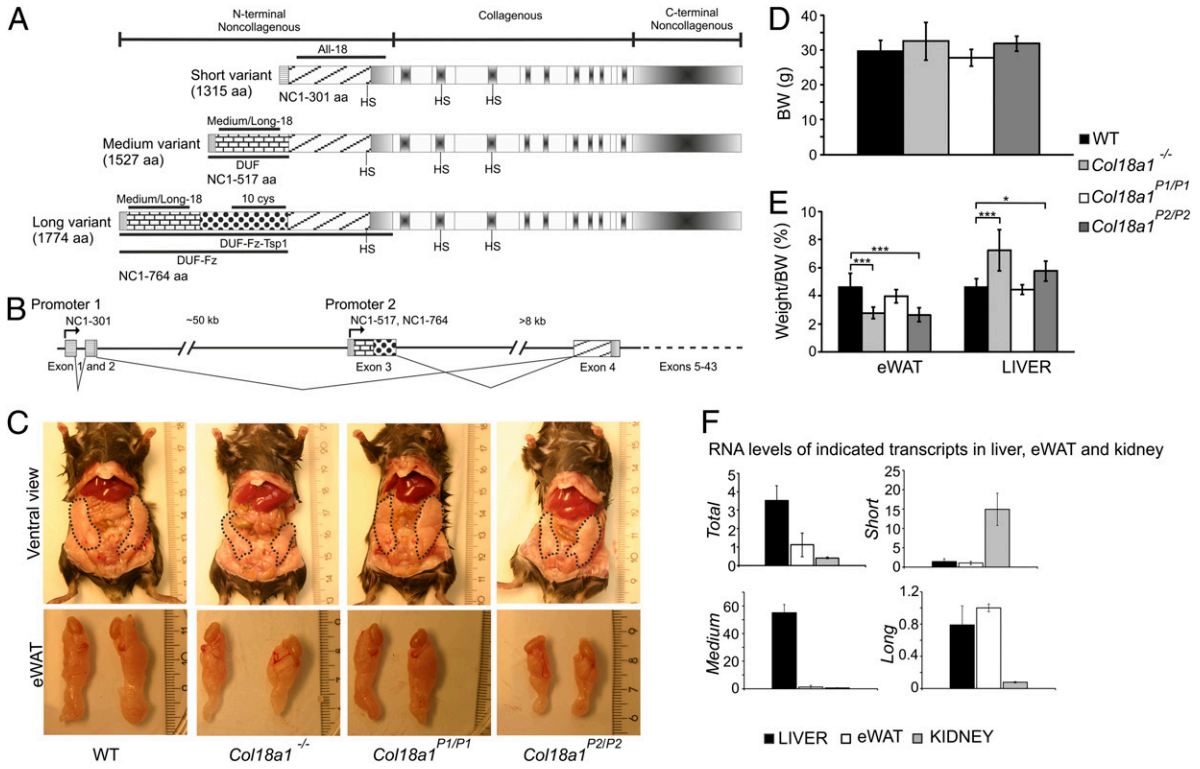

Fig. 1. Isoform-specific effects of collagen XVIII on BW, adiposities, and liver weights. (*A*) Horizontal and vertical stripes denote signal sequences of short (*Top*) and medium/long isoforms of mouse collagen XVIII, respectively. White and gray boxes depict collagenous and NC regions, respectively. Brick pattern denotes the DUF. Black dots denote the Fz homology domain containing 10 conserved cysteines (cys) followed by the Tsp1 homology domain depicted in diagonal stripes. Predicted HS attachment sites, recombinant fragments produced, and epitopes of the anti–all-18 and anti–medium/long-18 antibodies are shown. (*B*) Collagen XVIII isoforms derive from utilization of alternative promoters. Exons 1 and 2 are specific to the short variant. Exon 3 (subject to alternative splicing) encodes middle and long variants. Exons 5–43 (not shown) are common to all isoforms. (*C*) Specified 12-wk-old mice were fed a Western diet for 5 wks. Ventral views (*Upper*) and eWAT of representative mice. (*D*) BW of 12-wk-old, male WT ($n = 15$), *Col18a1*$^{-/-}$ ($n = 5$), *Col18a1*$^{P1/P1}$ ($n = 7$), and *Col18a1*$^{P2/P2}$ ($n = 5$) mice fed a Western diet for 5 wk. (*E*) Weights of eWAT (total mass of both fat pads) and livers of mice in *D*, expressed as percentage of BW. (*F*) Relative *Col18a1* RNA levels in liver, eWAT, and kidney of 12-wk-old WT mice fed standard chow were quantified by RT-qPCR. Data (mean ± SD), normalized to β-actin, are relative to eWAT. $^{*}P < 0.05$, $^{***}P < 0.001$.

suggesting that few, if any, stable collagen XVIII homotrimers are assembled from the truncated *Col18a1 P1*- and *P2*-derived transcripts (Fig. S2), as expected from structural data (20). Thus, collectively our data show that the strategy depicted in Fig. S1 successfully generated mice producing only short ($Col18a1^{P2/P2}$) or medium/long ($Col18a1^{P1/P1}$) collagen XVIII (Fig. 1*B*), and at levels comparable to the WT animals (Fig. S2), whereas the $Col18a1^{-/-}$ mice produced neither.

Reanalysis of $Col18a1^{-/-}$ mice identified two previously unrecognized consequences of total collagen XVIII deficiency: generalized reduction in adiposity, observed on both Western (Fig. 1 *C* and *E*) and standard diets (Fig. S4), and a percentage of their body weight (BW) (Fig. 1*D*) increased liver weights on the Western diet (Fig. 1*E*). *P1*- and *P2*-null mice displayed no gross phenotypic alterations, were fertile, and had normal lifespans. However, adult *P2*-null mice had reduced adiposity (Fig. 1 *C* and *E* and Fig. S4) and increased liver weight (Fig. 1*E* and Fig. S4). No such changes developed in $Col18a1^{P1/P1}$ mice on a Western diet (Fig. 1 *C*–*E*), although they were lighter on chow (Fig. S4). However, despite reduced adiposities, $Col18a1^{-/-}$ and *P2*-null mice had adipocytes of comparable sizes to WT animals (Fig. S5).

We quantified by RT-qPCR, *P1*- and *P2*-derived transcript levels in the two tissues macroscopically affected in $Col18a1^{-/-}$ and $Col18a1^{P2/P2}$ mice. Primers that amplify all three RNA species indicate that the liver and eWAT of WT mice contain 8.5- and 2.7-fold more *Col18a1* RNA than kidney (Fig. 1*F*, *Upper Left*). Although, the use of isoform-specific primers precludes exact comparisons of the relative levels of each *Col18a1* transcript in any one tissue, it is evident that *P1*-derived RNA encoding short collagen XVIII predominated in the kidney (Fig. 1*F*, *Upper Right*). In comparison, *P2*-derived transcripts encoding the medium isoform were the majority species in the liver (Fig. 1*F*, *Lower Left*), and in this organ it was 90- and 55-fold more abundant than in kidney and eWAT, respectively. The longer *P2*-derived transcript was present at comparable levels in liver and eWAT, and at much higher levels than kidney (Fig. 1*F*, *Lower Right*). This transcript was also selectively up-regulated in eWAT of mice fed a short-term, high-fat diet (Table S1). Thus, taken together our data suggest that *P2*-derived *Col18a1* gene-products conduct key functions in WAT and liver.

Isoform-Specific Contributions of Collagen XVIII Variants to WAT Development. FACS of eWAT samples from mutant mice revealed that relative to WT and *P1*-null samples, eWAT from $Col18a1^{-/-}$ and *P2*-null mice contained significantly bigger pools of the cell population (i.e., $Lin^-/CD29^+/CD34^+/Sca\text{-}1^+/CD24^+$) enriched in early adipocyte progenitors (21) (Fig. 2*A*), whereas immunofluorescent staining studies with the anti–medium/long-18 and CD31 antibodies showed that *P2*-derived *Col18a1* products reside between adipocytes and within the vasculature (Fig. 2*B*, first panel). Thus, the anti–medium/long-18 antibody produced no staining in the $Col18a1^{-/-}$ samples (Fig. 2*B*, second panel), whereas the pattern and strength of staining of $Col18a1^{P1/P1}$ eWAT (Fig. 2*B*, third panel) were similar to WT; it also produced no or minimal staining with $Col18a1^{P2/P2}$ samples (Fig. 2*B*, fourth panel). In contrast, the anti–all-18 antibody returned some staining around adipocytes and within vessels of *P2* samples, indicating presence of short collagen XVIII (Fig. S6). Critically, the level of *P1*-derived *Col18a1* RNA in the eWAT of these mice was not increased to compensate for loss of *P2*-derived products (Fig. S2*D*). Moreover, as judged by the comparable distribution of $CD31^+$ blood vessels among genotypes, angiogenesis in the WAT of the $Col18a1^{-/-}$ and *P2*-null mice was not impaired (Fig. 2*B* and Fig. S6). The lack of medium/long collagen XVIII species in eWAT of these mice was confirmed by Western blotting (Fig. 2*C*), and incubations of WT and *P1*-null samples with heparitinase I established that medium/long collagen XVIII contain heparin sulfate (HS) side-chains (Fig. 2*C*, *Right*).

We profiled younger mice to gain insights into the role of medium/long collagen XVIII in WAT accrual. On standard chow, 4- to 6-wk-old $Col18a1^{P1/P1}$ mice had lower BWs than age-matched control animals, but they did not have decreased adiposities (Table S2), independently replicating the findings in mature mice (Fig. S4). Standard histological staining of eWAT samples also revealed no reductions in adipocyte size (Fig. 2 *D* and *E*). In contrast, 4-wk-old $Col18a1^{-/-}$ and *P2*-null mice displayed reduced adiposities (Table S2) and, in contrast to mature mice (Fig. S5), had smaller adipocytes than age-matched WT and *P1*-null animals (Fig. 2 *D* and *E*). This size difference diminished with age, such that by 7 wk of age $Col18a1^{-/-}$ and *P2*-null mice had adipocytes of comparable size to their WT and *P1*-null littermates (Fig. 2 *D* and *E*), despite continuing reduced adiposities (Table S2). Hence these data, plus the finding of a significantly larger adipocyte progenitor cell population within the eWAT of ∼4-wk-old mice (Fig. 2*A*), suggest that the origin of reduced adiposities in $Col18a1^{-/-}$ and *P2*-null mice (Fig. 1 *C* and *E*, Fig. S4, and Table S2) is complex, potentially involving defects at the adipocyte progenitor cell stage, a delay in the enrolment of preadipocytes into an adipogenic differentiation program (21–24), and enhanced dedifferentiation of adipocytes (25).

Reciprocal Regulation of *P1*- and *P2-Col18a1* Transcripts During Differentiation and Dedifferentiation. To explore the potential contribution of medium/long collagen XVIII to adipocyte differentiation, we used 3T3-L1 cells, a well-characterized mouse embryo-derived preadipocyte differentiation model (24, 26). *Col18a1* RNA levels rose ∼fourfold during differentiation (Fig. 3*A*, first panel, *Upper*) as a result of marked rises in *P2*-derived transcript numbers. Thus, before differentiation (0 h), *P1*-derived *Col18a1* transcripts were the predominant species, and *P2* transcripts encoding medium collagen XVIII were the least abundant (Fig. S7). Four days following induction of differentiation, *P1*-derived RNA levels fell dramatically (Fig. 3*A*, second panel, *Upper*), and *P2*-transcripts increased strongly (Fig. 3*A*, third and fourth panels, *Upper*). These changes were paired with a marked fall in *Wnt10b* RNA (Fig. 3*A*, fifth panel, *Upper*), which encodes a potent adipogenic inhibitor (27, 28); increased RNA levels of peroxisome proliferator-activated receptor-γ (*Pparγ*) (Fig. 3*A*, *Lower Left*), encoding a key adipogenic transcription factor (29); and of the *PPARγ* target, adipocyte protein 2 (*aP2*) (Fig. 3*A*, *Lower Right*) (30). Complementing the RNA data, the anti–medium/long-18 antibody stained induced 3T3-L1 cells much more strongly than noninduced cells (Fig. 3*B*). Moreover, as shown for Wnt3a (18), recombinant DUF/Fz collagen XVIII sequences (Fig. 1*A*) pulled-down Wnt10b in vitro (Fig. 3*C*, *Right*), and to a far greater extent than the equivalent protein lacking the Fz domain (Fig. 3*C*). Thus, these data—plus the profiling of younger mice (Fig. 2 *D* and *E* and Table S2)—suggest that sequences unique to medium and long collagen XVIII support preadipocyte differentiation.

To determine if medium/long collagen XVIII sequences might also contribute to adipocyte dedifferentiation, we incubated differentiated 3T3-L1 cells in Wnt3a-conditioned medium (CM). This process produced the expected signs of dedifferentiation, such as a marked decrease in the number and size of lipid droplets (not shown) and reduced levels of *PPARγ* and *aP2* RNA (Fig. 3*D*). The levels of medium and long *Col18a1* RNA fell, but *P1*-derived *Col18a1* RNA rose (Fig. 3*D*). Thus, these results, and the finding that the Fz-sequences of collagen XVIII (Fig. 1*A*) sequester Wnt3a (18, 31), suggest that *P2*-derived gene-products may inhibit rather than support adipocyte dedifferentiation.

To substantiate the in vivo (Fig. 2*A* and Table S2) and in vitro (Fig. 3 *A*–*D*) data that lack of medium/long collagen XVIII would reduce the number of precursor cells attaining or maintaining a fully differentiated adipogenic state, we cultured

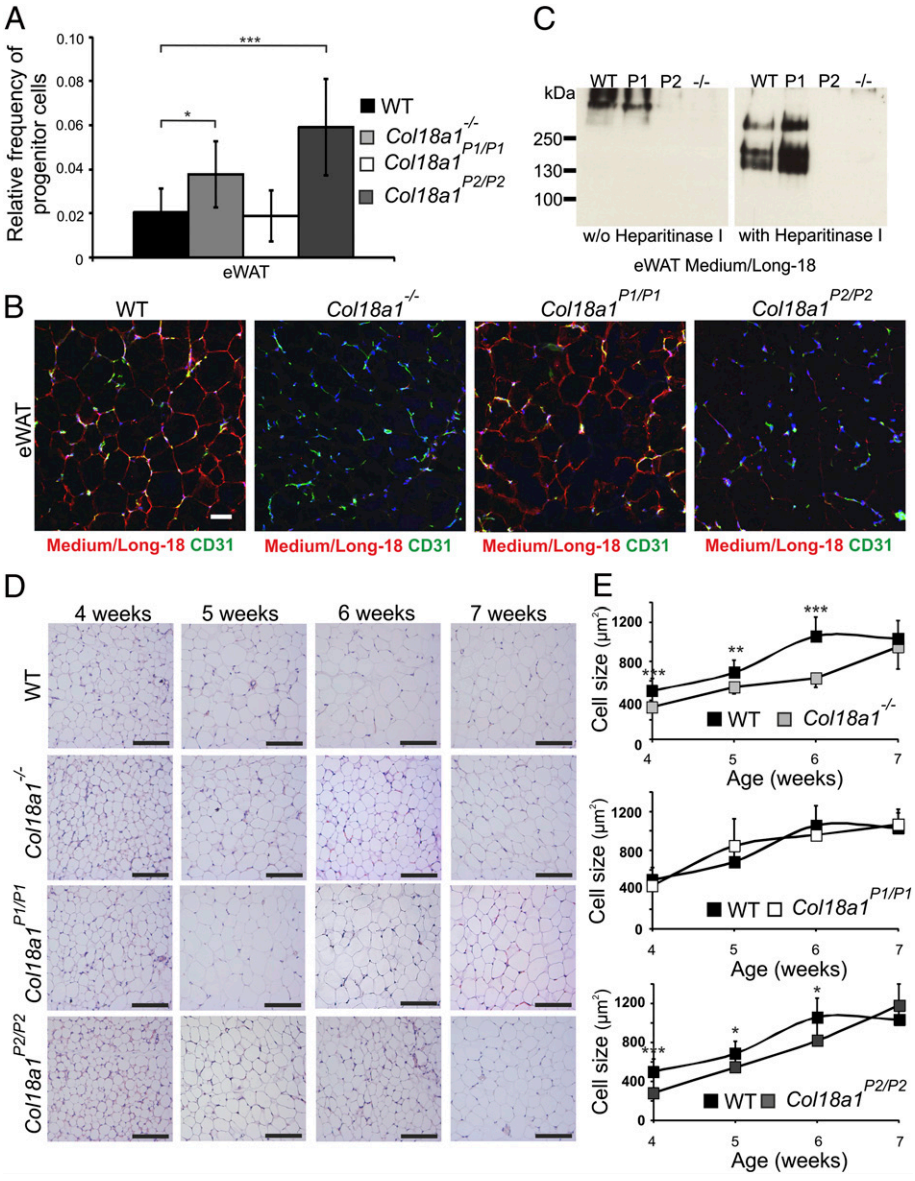

Fig. 2. Collagen XVIII variants contribute to the composition and development of WAT. (*A*) Percentages of the Lin^-:$CD29^+$:$CD34^+$: $Sca1^+$:$CD24^+$ cell subpopulation, enriched in early adipocyte progenitors, in eWAT of 22- to 26-d-old male mice fed standard chow: WT (n = 11), *Col18a1*$^{-/-}$ (n = 6), *Col18a1*$^{P1/P1}$ (n = 6), and *Col18a1*$^{P2/P2}$ (n = 10). (*B*) Immunostaining of extracellular matrix of adipocytes and vasculature with anti–medium/long-18 (red) and anti-CD31 (green) antibodies, respectively. The yellow fluorescence indicates colocalization of medium/long collagen XVIII isoforms with $CD31^+$ blood vessels. Samples from 12-wk-old mice fed a Western diet for 5 wk. (Scale bar, 100 μm.) (*C*) Western blots of eWAT cell homogenates from specific mice without (w/o) and with heparitinase I treatment. The distinct immunoreactive products in heparitinase I-treated samples indicate that medium/long collagen XVIII contains HS chains. Estimated sizes of medium and long collagen XVIII isoforms are respectively 156 and 182 kDa, but collagens run anomalously on SDS/PAGE. (*D*) Representative images of H&E-stained eWAT from specified male mice on standard chow at specified ages. (Scale bars, 100 μm.) (*E*) Mean adipocyte sizes of eWAT from age-matched WT and mutant mice reared on standard chow. All cells in two to five microscopic fields per sample were counted at each weekly time point. Error bars show SD calculated from ≥3 mice. $*P < 0.05$, $**P < 0.01$, $***P < 0.001$.

murine embryonic fibroblasts (MEF) from the WT and mutant animals. Before addition of the adipogenic stimuli, collagen XVIII was detectable only in WT and *P2*-null MEFs (Fig. 3*E*), indicating that short collagen XVIII is the major species produced in this undifferentiated cell type, similar to 3T3-L1 cells (Fig. 3*A* and Fig. S7). RT-qPCR showed that 8 d after induction, *P2*-derived transcripts were 2.8- (medium) and 3.1- (long) fold higher in WT cultures, compared with 1.6-fold for *P1*-RNA (data from two independent experiments). As judged by cell morphology and Oil-red O staining, MEF cultures contained heterogeneous populations of cells, with the numbers of fully differentiated adipocytes varying from experiment to experiment.

Cultured *P1*-null MEFs contained Oil-red O-stained cells at a level comparable to WT cultures, when challenged by an adipogenic differentiation cocktail (Fig. 3 *F* and *G*). In comparison, in each of three independent experiments, fewer *Col18a1*$^{-/-}$ and *P2*-null MEFs attained/maintained the characteristics of mature adipocytes (Fig. 3*F*), and mean levels of Oil-red O staining (Fig. 3*G*), *Pparγ* (Fig. 3*H*), and *aP2* (Fig. 3*I*) RNAs were all reduced. Thus, these data (Fig. 3 *E*–*I*) and previous work (18, 25) suggest that the reduced adiposities of *P2*-null and *Col18a1*$^{-/-}$ mice (Fig. 1*C* and Table S2) stem, at least in part, from fewer precursor cells attaining/maintaining a fully differentiated adipogenic state, and that collagen XVIII–DUF/Fz sequences inhibit Wnt-signaling in pre- and mature adipocytes.

Reciprocal Relationship Between *P1*- and *P2-Col18a1* Transcripts in Abdominal Visceral Fat. We also compared *P1*- and *P2*-derived *COL18A1* transcript levels in visceral and subcutaneous fat using WAT samples from 102 participants undergoing Roux-en-Y gastric bypass surgery (32). Total *COL18A1* RNA was comparable in these two depots (Fig. S8). However, relative to subcutaneous fat, visceral fat contained proportionally more *P2*-derived species and fewer *P1*-transcripts (Fig. S8) (all $P < 0.001$ for differences from subcutaneous fat). Moreover, whereas *P1*-derived *COL18A1* RNA levels in subcutaneous and visceral fat samples displayed no correlation with serum free fatty acid levels, the levels of *P2*-derived RNA in visceral fat samples did (Spearman correlation, $P < 0.01$).

Medium/Long Collagen XVIII Isoform Line Liver Sinusoids and Bind ApoE. Because free fatty acids released from abdominal visceral fat directly accesses the liver via the portal vein, and mice

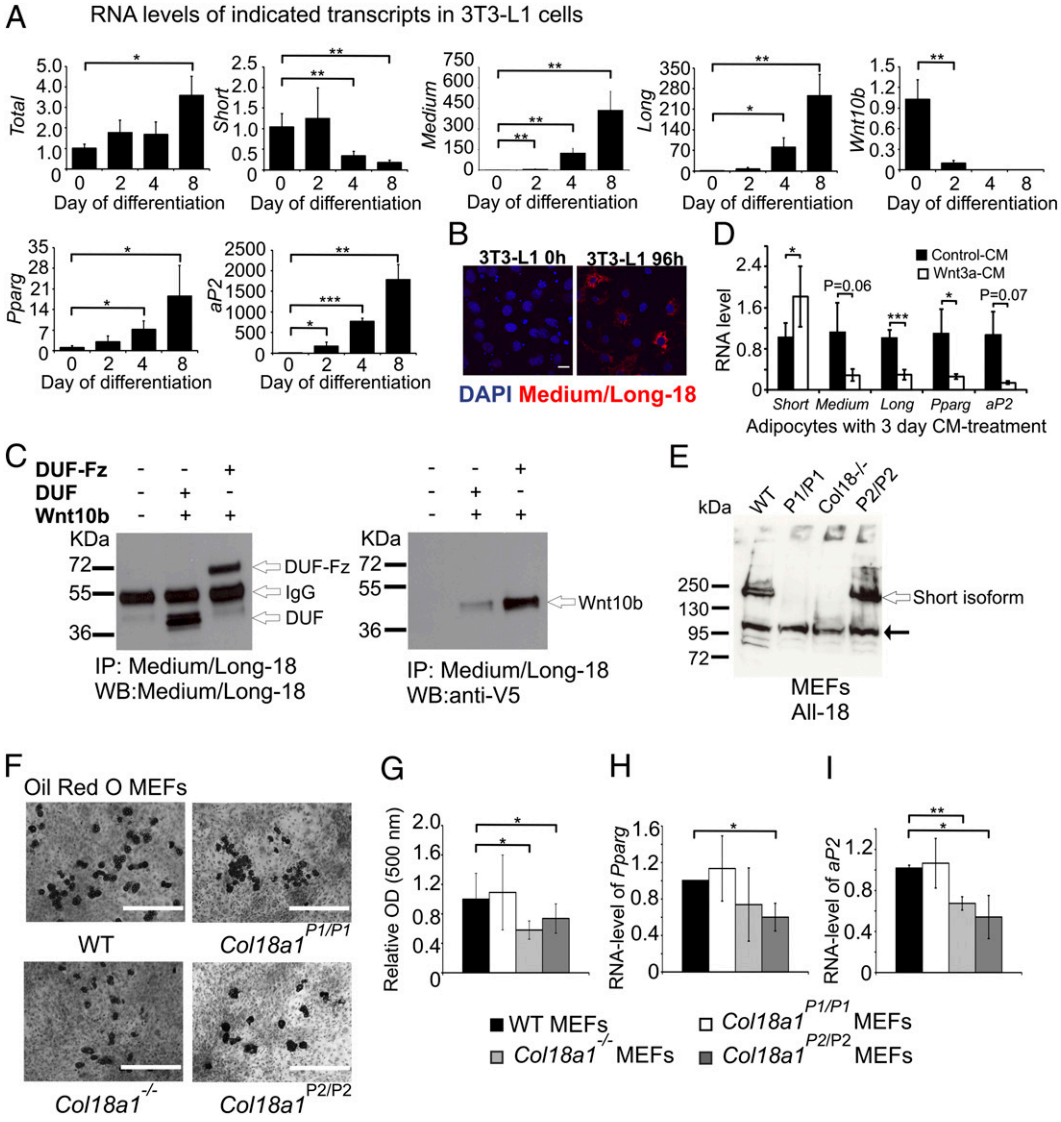

Fig. 3. Medium/long collagen XVIII isoforms promote an early stage of adipogenesis. (*A*) Postconfluent 3T3-L1 cells (assigned day 0) were induced to differentiate as described in *Methods*. Transcripts were quantified by RT-qPCR. Values (mean ± SD), normalized to 18s rRNA and relative to 0 h, are from two independent experiments performed in duplicate. (*B*) Confocal images of 3T3-L1 cells stained with the anti–medium/long-18 antibody (red). Nuclei counterstained with DAPI (blue). (Scale bar, 100 μm.) (*C*) HEK293 cells expressing the N termini of either medium (lane 2) or long (lane 3) collagen XVIII (Fig. 1*A*) and Wnt10b-V5 were harvested by scraping into native lysis buffer. Immunoprecipitation (IP) and Western blot (WB) analysis were performed with specified antibodies. (*D*) 3T3-L1 cells were induced to differentiate, and at day 10 of differentiation the cells were treated for 3 d with either 10% (vol/vol) Wnt3a-CM, to induce dedifferentiation, or 10% (vol/vol) Ctrl-CM. Transcript levels were quantified by RT-qPCR. (*E*) Western blot of MEFs homogenates from WT and mutant mice. Note, *P1*-derived *Col18a1* gene-product is the predominate isoform in undifferentiated MEFs. Black arrow indicates a nonspecific immunoreactive product. (*F*) Oil-red O staining of representative cultures of MEFs incubated with adipocyte differentiation media for 8 d. (Scale bars, 400 μm.) (*G*) Histograms show Oil-red O content of differentiated MEF cultures (two to four embryos per genotype). Values (mean ± SD) expressed relative to WT are from three independent experiments. (*H* and *I*) *Pparg* and *aP2* RNA levels were quantified by RT-qPCR. MEFs were incubated with adipocyte differentiation media for 8 d. Values (mean ± SD) normalized to 18s rRNA and relative to WT are from two ($Col18a1^{-/-}$) or three (all other lines) independent experiments. $^{*}P < 0.05$, $^{**}P < 0.01$, $^{***}P < 0.001$.

lacking medium/long collagen XVIII develop a liver phenotype (Fig. 1 *C* and *E* and Fig. S4), we examined the microanatomy of this organ in more detail. Hepatocytes from $Col18a1^{-/-}$ and *P2*-null mice tended to contain more lipid and apoE than WT and *P1*-null samples (Fig. 4*A* and Fig. S9), indicating that loss of medium/long collagen XVIII did not impair hepatic free fatty acid uptake or apoE-mediated internalization of chylomicron and VLDL remnants (33, 34). The anti–all-18 antibody produced comparable staining signals in WT and *P1*-null mice livers, but only stained the portal regions of *P2*-null mice livers (Fig. 4*B*). Thus, these analyses, plus the RNA data (Fig. 1*F*), indicate that medium collagen XVIII is the most abundant isoform in hepatic sinusoids. Moreover, in *P2*-null mice there is minimal, if any, compensatory rise in production of the short isoform (Fig. S2).

Immunoelectron microscopy studies using the anti–medium/long-18 antibody identified immunoreactive products in the Space of Disse, evenly distributed between hepatocytes and endothelial cells (Fig. 4*C*), indicating that medium/long collagen XVIII contributes to the discontinuous BM of the subendothelial space. Western blot analysis detected a smear of high molecular-weight immunoreactive products, which disappeared on incubation with heparitinase I but

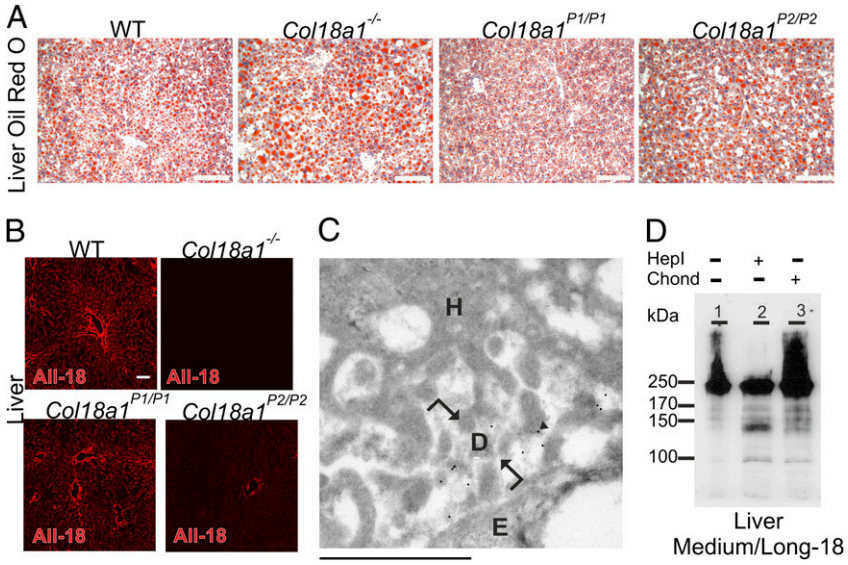

Fig. 4. Hepatic lipid accumulation in mice lacking collagen XVIII in the Space of Disse. (*A*) Livers were excised from 12-wk-old mice after 5 wk on a Western diet and stained with Oil-red O. Representative samples from WT and mutant mice. (Scale bars, 100 μm.) (*B*) Collagen XVIII staining of the portal regions and sinusoidal spaces lining hepatocytes of WT and *Col18a1*$^{P1/P1}$ mice livers. Staining is restricted to portal region of *Col18a1*$^{P2/P2}$ livers. (Scale bar, 100 μm.) (*C*) Immunoelectron microscopy analyses of WT sample with the anti–medium/long-18 antibody localizes medium/long collagen XVIII to the Space of Disse. H, hepatocyte; D, Space of Disse; E, endothelial cell; arrowhead, immunogold particle. (Scale bar, 1 μm.) (*D*) Enzymatic digestion of WT mouse liver homogenate. Lane 1, undigested. Heparitinase I (HepI) (lane 2) and chondroitinase ABC (Chond) (lane 3) digested. Product sizes are not directly comparable to those in eWAT (Fig. 2*C*) because of tissue-specific differences in isoform expression and conditions of the SDS/PAGE analysis.

not chondroitinase ABC (Fig. 4*D*). Thus, these data indicate that sinusoidal collagen XVIII contains HS side-chains.

Immunofluorescent staining of WT liver revealed possible colocalization of sinusoidal medium/long collagen XVIII with apoE (Fig. 5 *A*–*C*). The anti–medium/long-18 antibody pulled down an immunoreactive product of the expected size of apoE (34 kDa) from WT but not *Col18a1*$^{P2/P2}$ homogenates (Fig. 5*D*), and in an ELISA, recombinant DUF-Fz-thrombospondin 1 (Tsp1) collagen XVIII sequences (Figs. 1*A* and 5*E*) bound apoE in a concentration and HS-dependent manner (Fig. 5*F*). Thus, collectively these data suggest that the binding between medium/long collagen XVIII and apoE within hepatic sinusoids is mediated through HS-modified, N-terminal NC sequences. Additionally, the loss of this interaction in *Col18a1*$^{-/-}$ and *P2*-null mice may contribute to their observed liver phenotypes (Figs. 1 *C* and *E* and 4*A*).

Col18a1$^{P2/P2}$, but Not Col18a1$^{P1/P1}$, Mice Develop Metabolic Abnormalities. The reduced adiposities and liver phenotypes of *P2*-null and *Col18a1*$^{-/-}$ mice (Figs. 1 *C* and *E*, 4*A*, and 5*D*) obliged us to undertake lipid and lipoprotein analyses. *Col18a1*$^{P1/P1}$ mice had a comparable blood lipid profile to WT animals (Fig. 6 *A* and *B* and Fig. S10 *A* and *B*), whereas *P2*-null mice had ∼70% higher

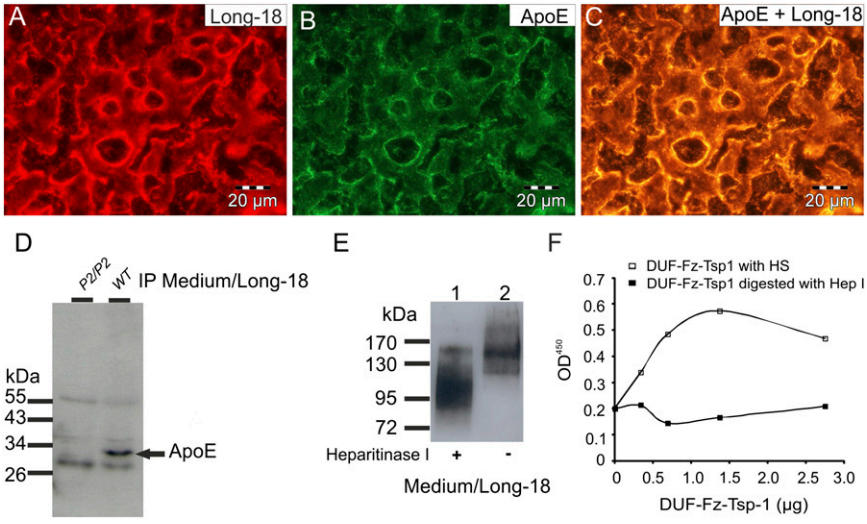

Fig. 5. Hepatic collagen XVIII interacts with ApoE. (*A*–*C*) Immunofluorescence was performed on livers from WT mice with specified antibodies. Colocalization is indicated by the overlay (yellow color). (Scale bars 20 μm.) (*D*) *Col18a1*$^{P2/P2}$ and WT liver homogenates were incubated with the anti–medium/long-18 antibody. Western blot of immunoprecipitated products (IP) using an anti-apoE antibody. (*E*) Recombinant DUF-Fz-Tsp1 (Fig. 1*A*) purified from HEK293 cell media. Lane 1, digested with heparitinase I. Lane 2, undigested. (*F*) Binding of recombinant DUF-Fz-Tsp1 to immobilized apoE3 was quantified using anti–medium/long-18 and HRP-conjugated secondary antibodies. Data are from a representative experiment.

serum triglyceride levels (Fig. 6*A*, Fig. S10*A*, and Table S3). Cholesterol levels were not increased (Fig. 6*B*, Fig. S10*B*, and Table S3). On standard chow, *Col18a1*$^{-/-}$ mice had less marked hypertriglyceridemia than *P2*-null mice (Fig. 6*A*) and no triglyceride phenotype on a Western diet (Fig. S10).

The hypertriglyceridemia of the *P2*-null mice was paired with increased VLDL triglyceride levels (Fig. 6*C* and Fig. S10). However, this finding was not attributable to reduced lipoprotein lipase activity in postheparinized plasma: activity levels in male *P2*-null and WT samples of free fatty acid were 17.6 ± 3.6 and 15.6 ± 2.4 μmol·mL·h, respectively; and in female mice the corresponding values for free fatty acid were 18.0 ± 3.7 and 14.7 ± 2.5 μmol·mL·h. Activity levels of hepatic lipase, a facilitator of hepatic uptake of high-density lipoprotein (HDL), and of chylomicron and VLDL remnants (35–37), were also not reduced: values of free fatty acid in male *P2*-null and WT mice were 11.9 ± 2.0 and 10.6 ± 1.6 μmol·mL·h, respectively, and the free fatty acid in the females was 10.7 ± 2.7 and 11.7 ± 1.6 μmol·mL·h (both not significant).

The increased VLDL-triglyceride levels in the *P2*-null mice could also not be ascribed to increased activity levels of phospholipid transfer protein (PLTP), known to increase VLDL secretion and the production of less-dense HDL particles (38, 39). PLTP activities in male *P2*-null and WT mice were 13,019 ± 1,190 and 16,212 ± 799 nmol·mL·h ($P < 0.01$ for difference), respectively. Similarly, female *P2*-null mice had lower, rather than increased, PLTP activity (10,523 ± 1,534 vs. 16,137 ± 3,000 nmol·mL·h in WT mice, $P < 0.01$ for difference). Thus, collectively our data suggest that the hypertriglyceridemia of *Col18a1*$^{-/-}$ and *P2*-null mice develops because of an imbalance between adipocyte differentiation and dedifferentiation (Fig. 3).

Discussion

The morphological and functional maturation of WAT is a complex process. First, mesenchymal cell precursors commit to becoming preadipocytes, which may then differentiate into fat-laden adipocytes (40). Second, adipocytes may dedifferentiate, thereby regaining their proliferative capacity (25). Herein, we demonstrate that the eWAT of mice genetically engineered to lack collagen XVIII–DUF/Fz sequences contained a larger reservoir of a cell population enriched in early adipocyte progenitors, and that MEFs from these animals have reduced adipogenic capacity, as judged by fewer cells attaining/maintaining a fully differentiated state upon culture in an adipogenic mixture. We also found that medium/long collagen XVIII expression markedly rises during the differentiation of 3T3-L1 preadipocytes to mature adipocytes (Fig. 3 *A* and *B* and Fig. S7), and that these increases coincide with a dramatic fall in *P1* RNA (short isoform) (Fig. 3*A* and Fig. S7). Conversely, inducing Wnt3a-mediated dedifferentiation of mature 3T3-L1 adipocytes produced marked falls in medium and long *Col18a1* RNA, and a rise in short transcript levels. Mirroring previous Wnt3a data (18, 31), we also show that collagen XVIII–DUF/Fz sequences bind the potent adipogenic inhibitor, Wnt10b in vitro. Taken together, our results indicate that collagen XVIII's DUF/Fz sequences support the differentiation of adipogenic progenitors, as well as the maintenance of the differentiated state. Furthermore, an imbalance between adipocyte differentiation and dedifferentiation helps explain the liver and lipid abnormalities that ensue in mice lacking these sequences.

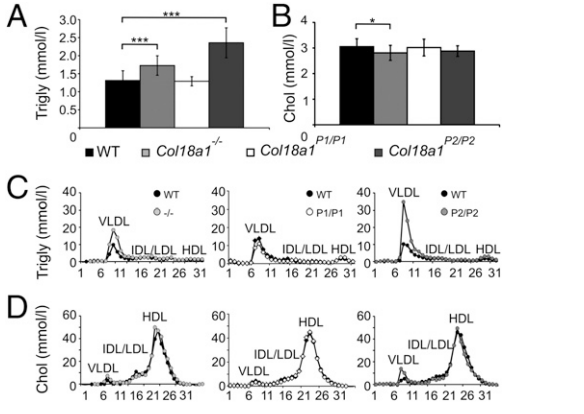

Fig. 6. Mice deficient for medium/long collagen XVIII have abnormal lipid and lipoprotein profiles. (*A* and *B*) Data are from ~8-wk-old male mice reared on standard chow. Fasting serum triglyceride (Trigly) (*A*) and cholesterol (Chol) (*B*) in WT ($n = 18$), *Col18a1*$^{-/-}$ ($n = 10$), *Col18a1*$^{P1/P1}$ ($n = 7$), and *Col18a1*$^{P2/P2}$ ($n = 5$) mice. (*C* and *D*) Lipoproteins in pooled serum from the specified mice were analyzed by FPLC gel-filtration, and the amounts of Trigly (*C*) and Chol (*D*) in each fraction determined. *$P < 0.05$, ***$P < 0.001$.

The proposition that collagen XVIII–DUF/Fz sequences support preadipocyte differentiation fits well with the recent findings of Park et al. (24). In essence, the authors established that 3T3-L1 preadipocytes irreversibly commit to an adipocyte fate early on in the differentiation process, coincident with attainment of a high PPARγ state and well before cytologically evident fat accumulation. Furthermore, the control of this switch (commitment) is under mixed regulation (which can include glucocorticoids and cAMP stimuli), with only minor contribution from insulin. In contrast, following commitment, insulin-signaling dominates and tightly regulates the individual cellular accumulation of fat. Here, we confirmed that glucocorticoid induction of 3T3-L1 preadipocytes increased *Pparγ* and produced the expected drop in *Wnt10b* RNA (41), and moreover showed that the timings of the dramatic rises in *P2*-derived *Col18a1* transcript levels (and precipitous fall of *P1*-derived RNA) mirrored those of *Pparγ* (Fig. 3*A*), consistent with the notion that it is only the medium/long collagen XVIII isoforms, and not the short form, that positively contribute to the mix of regulatory factors controlling recruitment of 3T3-L1 cells to an adipogenic differentiation program. We also found that despite their reduced adiposities (Fig. 1 *C* and *E* and Fig. S4), adult *P2*-null mice (who do not produce collagen XVIII–DUF/Fz sequences) had comparable sized adipocytes to equivalently fed WT mice (Fig. 2 *E* and *F* and Fig. S5), again indicating that individually committed *Col18a1*$^{P2/P2}$ preadipocytes had the same capacity to accumulate lipid as committed WT and *P1*-null preadipocytes and that the attainment of this committed state is aided by medium/long collagen XVIII species.

Previous studies have made good progress in documenting the changes in Wnt expression that accompany adipogenesis (27, 41), and their mechanisms of signaling through cell-surface Fz receptors (42). For example, it has been shown that *Wnt10b*—but not *Wnt3a*—RNA is present at a relatively high level in human mesenchymal precursor cells (27) and preadipocytes (41), and that *Wnt10b* RNA levels fall quite dramatically in these cell types following addition of adipocytogenic mixtures (43). Conversely, enforced Wnt10b expression in ST2 marrow-derived stromal cells (44) and 3T3-L1 preadipocytes suppresses adipocyte differentiation and lowers *Pparγ* RNA, even before adipogenesis is induced (41, 43). Moreover, high-level *Wnt10b* expression in transgenic mice reduces both *Pparγ* expression and WAT development but not adipocyte size (45). It has also been shown that Wnt10b inhibits preadipocyte differentiation via activation of Fz receptors 1 and 2 (42), and that collagen XVIII-derived Fz sequences suppress Wnt3a-activated signaling through its extracellular decoy receptor activity (18, 31). Here we show that any sequestering of Wnt10b and of other secreted Wnt inhibitors of adipogenesis (41) by this decoy receptor is likely to be minimal in 3T3-L1 preadipocytes and undifferentiated MEFs because of their inherently low level of long collagen XVIII expression (Fig. 3 *A*, *B*, and *E* and Fig. S7), and also note that sequestering

of these inhibitors via collagen XVIII-generated DUF/Fz sequences cannot occur in *P2*-null mice. Importantly, we further show that a significant lowering of *P2* (*P1* increased) -derived *Col18a1* gene-products forms part of a regulatory system mediating Wnt3a-induced dedifferentiation of adipocytes (Fig. 3*D*), reinforcing the notion that reduced sequestration of Wnt3a and other Wnt molecules via collagen XVIII's DUF/Fz decoy activity could serve to maintain/restore an undifferentiated state, all other factors being equal. In this regard, we recognize that these decoy sequences do not contain a HS attachment site (Fig. 1*A*) and, as such, that the reduced adiposity of *P2*-null animals is unlikely to be directly attributable to the loss of collagen XVIII-mediated HS signaling activities, especially as *P2*-derived *Col18a1* gene-products make very modest contributions to the extracellular collagen XVIII contents of undifferentiated MEFs (Fig. 3*E*) and preadipocytes.

The observation that eWAT of 22- to 26-d-old male *P2*-null mice tended to have a larger reservoir of a cell population enriched in early adipocyte progenitors than *Col18a1*$^{-/-}$ mice (Fig. 2*A*) fits well with our data, which strongly indicate that *P1*- and *P2*-derived *Col18a1* gene products play reciprocal roles in the processes controlling the commitment of undifferentiated cells to an adipogenic state (Fig. 3 *A*, *B*, and *F*), and of the subsequent processes maintaining the differentiated state (Fig. 3*D*). Specifically, the data suggest a model whereby the selective absence of medium/long collagen XVIII species (i.e., as occurs in *P2*-null mice) creates a cellular environment more conducive to progenitor cell proliferation than differentiation, whereas total absence of collagen XVIII produces two opposing environments: one that is conductive for early adipocyte progenitor differentiation (rather than proliferation) because of lack of short collagen XVIII expression, and one that helps maintain the undifferentiated state because of the absence of medium/long collagen XVIII species.

With respect to the counterintuitive finding that only *P2*-null mice had higher serum triglyceride levels than WT on a high-fat diet (Fig. S10), we note that the liver weights of the *P2*-null mice (as a percentage of their BW) tended to be lower than those of equivalently aged (i.e., 12 wk) and fed *Col18a1*$^{-/-}$ mice (Fig. 1*E*), whereas ∼8-wk-old *P2*-null mice fed standard chow tended to have slightly higher, rather than lower, liver weights than *Col18a1*$^{-/-}$ animals (Fig. S4*B*). Hence, it is tempting to speculate that the more pronounced increase in the liver weights of the high-fat diet fed *Col18a1*$^{-/-}$ mice (versus *P2*-null) (Fig. 1*E*) may be ascribed, at least in part, to increased uptake of apoE-containing lipoproteins, such as VLDL (Fig. S9), especially as the livers of these mice contained more lipid than WT mice (Fig. 4*A*), and this was paired with normalization of their serum triglyceride levels (Fig. S10) plus continued reduced adiposity (Fig. 1*E*). The implication, which seems entirely consistent with studies on apoE-lipoprotein clearance in liver (33, 34) and this study's observation that N-terminal HS-modified collagen XVIII species interact with apoE (Fig. 5*F*), is that collagen XVIII serves to delay the clearance of triglyceride-rich lipoproteins by binding/sequestering apoE, and therefore total ablation of collagen XVIII in the liver sinusoidal space is more consequential than the lack of only the medium/long isoforms, particularly in the setting of a primary defect in adipogenesis.

Results from a recent microarray study (46) add further credence to the proposition that sinusoidal collagen XVIII contributes to hepatic triglyceride homeostasis. In short, it turns out that hepatic *XBP1* ablation lowered serum triglyceride levels and that this was attributable to activation of a feedback mechanism that lowered not only *Dgat2* (triglyceride synthesis) and *Angplt3* (LPL inhibitor) mRNA levels, but also *Col18a1* transcripts. Thus, combining these data with the results of the present study suggest that restoring the deposition of collagen XVIII in the sinusoidal area of *P2*-null mouse livers would very likely reduce their susceptibility to steatosis (and potentially lipotoxicity), albeit at the expense of exacerbating their hypertriglyceridemia.

What of the clinical relevance? Tantalizingly, while this paper was in preparation, Peloso et al. (47) reported that the low-frequency *COL18A1* c.331G > A variant (predicted to encode p.Gly111Arg) (Fig. 1*A*, present in medium/long isoform) has a large effect of serum triglyceride levels (−16%; $P = 2 \times 10^{-16}$) and a marginal impact on HDL-C (2 mg/dL; $P = 4 \times 10^{-4}$). Complementing these results, human genetic linkage studies have returned robust statistical evidence of linkage between the chromosome 21 interval housing *COL18A1* and the Familial Combined Hyperlipidemia-Triglyceride trait (Fig. S11), and raised serum triglyceride and LDL-C in hypertensive pedigrees (48). Here, we have shown that *P2-COL18A1* transcript levels in visceral but not subcutaneous fat are positively correlated with serum free fatty acid concentrations (Fig. S8), and note that fatty acid uptake is ∼30% higher in visceral (on a gram to gram basis) than subcutaneous fat (49). We also found proportionally more *P2*-derived *COL18A1* RNAs and fewer *P1*-transcripts in visceral than subcutaneous fat of obese subjects, which—based on the results emanating from our *P2*-null mice studies—suggest that this fat depot contains more cells committing to adipogenesis and maintenance of the differentiated state. Thus, although additional studies are required to establish whether the *COL18A1* c.331G > A variant itself (or an allele in linkage disequilibrium) is responsible for the triglyceride-lowering effect, from the data presented herein it seems conceivable that *COL18A1* variants having a major deleterious impact on collagen XVIII's DUF/Fz sequences could cause atherogenic dyslipidemia and fatty liver, secondary to impaired adipogenesis. Furthermore, we note that factors regulating collagen XVIII expression may contribute to kidney health in later life by affecting the BM of proximal tubules (short isoform) and of glomerular podocyte foot processes (medium/long isoforms) (19). It may also be clinically relevant that short collagen XVIII is expressed widely in the BM of the retina, and that the retinal vessels of *P1*-, but not *P2*- mice develop the same vessel outgrowth abnormality seen in *Col18a1*$^{-/-}$ mice (50).

Methods

Generation of *P1*- and *P2*-Null Mice. All animal experiments were approved by the Laboratory Animal Centre of the University of Oulu, Oulu, Finland. To deplete *P1* transcripts, a targeting construct with a LacZ-Neo cassette was inserted in-frame into *Col18a1* exon 1. To deplete *P2* transcripts, an HSV-tk-neo^{r} selection cassette flanked by LoxP sequences were introduced downstream of exon 3. *SI Methods* and Table S4, respectively, provide further details on the generation of the *P1*- and *P2*- null lines and the primer sequences. The creation of the *Col18a1*$^{-/-}$ mouse line, which has been previously described (8), used a targeting vector (insertion site, exon 30) that interrupts all collagen XVIII variants (8). All mouse lines were bred into a C57BL/6JOlaHsd background (Harlan Laboratories) for at least seven generations and WT littermates were used as controls. All mice were maintained on a 12-h light/12-h dark cycle and fed ad libitum with standard chow [5% (wt/wt) fat] or a Western diet [0.2% cholesterol and 21% (wt/wt) fat].

Human Studies. Subcutaneous and visceral adipose tissue biopsies were collected from 102 morbidly obese participants of the ongoing Kuopio Obesity Surgery Study (32) undergoing Roux-en-Y gastric bypass surgery at Kuopio University Hospital (>90% participated). Clinical parameters including serum free fatty acid levels were assessed before the surgery. The study protocol was approved by the Ethics Committee of Northern Savo Hospital District and carried out in accordance with the Helsinki Declaration. Informed written consent was obtained from all participants.

RT-qPCR. RNA from snap-frozen mouse tissues, 3T3-L1 cells, or MEFs were isolated with Qiagen kits (QIAzol and RNeasy mini). cDNA was produced with the iScript cDNA synthesis kit (Bio-Rad). RT-qPCR was performed with iTaq SYBR Green Supermix with ROX reagents (Bio-Rad). All assays were performed in duplicate using a MX3005P QPCR system (Stratagene). Relative RNA levels were calculated by the $2^{\Delta\Delta Ct}$ method (51). Values were normalized

to β-actin or 18s rRNA. RNA from snap-frozen human subcutaneous and visceral adipose tissue biopsies was isolated and analyzed, as previously described (32). Tables S5 and S6 provide primer sequences.

Immunofluorescent Staining. Snap-frozen tissues were embedded in Tissue-Tek OCT Compound (Sakura Finetechnical). Cryosections (5 μm, kidney and liver, 10 μm, eWAT) were fixed in acetone and blocked with 1% BSA-PBS for 1 h at room temperature. Cells grown on cover-slips were fixed in 4% (wt/vol) paraformaldehyde–PBS and blocked for 1 h with 5% (vol/vol) normal goat serum-0.3% TritonX-100-PBS at room temperature. Sections were incubated for 24 h at 4 °C with the mouse anti–all-, anti–medium/long-18 (Fig. 1) (21), anti-mouse CD31 (BD Biosciences), or apoE antibodies (Santa Cruz Biotechnology), and then Cy3- or Alexa 488-conjugated secondary antibodies (Jackson ImmunoResearch Laboratories). Cell nuclei were visualized with 4′,6′-diamino-2-phenylindole hydrochloride (DAPI) (Sigma-Aldrich). Images were captured with an Olympus IX81 laser confocal microscope.

FACS and Morphometric Analysis of Adipose Tissue. eWAT was excised and analyzed as described previously (21, 52), with minor modifications. Tissues were minced in PBS and digested with collagenase (Worthington Biochemical Corporation) (1 mL/g of homogenized tissue) at 37 °C for 2 h. Cells were collected by centrifugation at 200 × *g* for 10 min, and the floating adipocyte layer and supernatant discarded. Red blood cells were lysed with PharmLyse buffer (BD Biosciences), washed in DMEM/F12, re-collected by centrifugation, and resuspended in PBS supplemented with 4% (vol/vol) FBS. The remaining stromovascular cells were passed through a 40-um cell strainer. For FACS, cells were incubated for 10 min with saturating concentrations of anti-mouse CD16/CD32 (Mouse Fc block, BD Biosciences) at room temperature, washed twice in PBS + 4% (vol/vol) FBS, and then incubated for 1 h at 4 °C with a mix of the following antibodies (BD Biosciences): APC Mouse lineage antibody mixture, PE-CD24, PE-Cy5-CD29, FITC-CD34, and Pe-Cy7-Ly-6A/E (Sca-1). Samples were acquired on a BD Biosciences FACSCalibur cytometer and CellQuest software. Analysis was performed with FlowJo software (Tree Star). For morphometric analysis, eWAT was fixed in 4% (wt/vol) paraformaldehyde–PBS for 24 h and embedded in paraffin. Deparaffinized sections (5 μm) were stained with H&E. Adipocyte size was determined using a Leica Microsystems microscope and ImageJ software (National Institutes of Health).

Western Blotting of eWAT and Liver Samples. Tissues were snap-frozen in liquid nitrogen, homogenized in PBS, and solubilized in 4× sample buffer [250 mM Tris·HCl, pH 6.8, 2 M urea, 8% (wt/vol) SDS, 0.01% bromophenol blue, 40% (wt/vol) glycerol, 4% (vol/vol) β-mercaptoethanol]. Samples were size-fractionated in denaturing SDS/PAGE followed by Western blotting for anti-medium/long antibody. Secondary antibodies were horseradish peroxidase-conjugated (Jackson ImmunoResearch Laboratories); detection was with Chemiluminescent Western blotting substrate (Amersham). Heparitinase I and chondroitinase ABC digestions were performed with 15-μL tissue homogenate (0.67mg of tissue per microliter of PBS) combined with 15 μL of 100 mM Tris-120 mM sodium acetate, pH 8.0, and 20 mU chondroitinase ABC (Sigma) or 15 μL PBS-3 mM $CaCl_2$, pH 7.0, and 5 mU heparitinase I (Seikagaku).

Differentiation of 3T3-L1 Cells and MEFs. The 3T3-L1 preadipocytes (ATCC-CL-173) were maintained in DMEM supplemented with 10% (vol/vol) BCS (ATCC). For differentiation, cells were grown to 2-d postconfluence and induced with a 3T3-L1 Adipocyte kit (Zen-Bio). Primary MEFs were isolated from mouse embryos at 13.5–15.5 d postcoitum; all experiments were performed with passage 2 or 3 cells. For differentiation, MEFs were split into six-well plates and cultured to confluence. Two days postconfluence, cell media were supplemented with 0.5 mM 3-Isobutyl-1-methylxanthine (Sigma-Aldrich), 1 μM dexamethasone, and 1 μg/mL insulin (Sigma-Aldrich) for 2 d, then 1 μg/mL insulin for 6 d. For Western blotting, cells were harvested in 1× native lysis buffer (Cell Signaling Technology). Oil-red O staining was performed with six parts 0.6% dye in isopropanol (Sigma-Aldrich) and four parts H_2O for 10 min. Excess stain was removed with H_2O. Retained Oil-red O was extracted with 100% isopropanol and quantified on a spectrophotometer at 500 nm.

Wnt3a-CM. Control (CRL-2648) and Wnt3a-expressing (CRL-2647) mouse L cells (ATCC) were cultured as described (25), and the resulting CM added to 3T3-L1 cells (10 d after initiation of differentiation) to a concentration of 10% (vol/vol).

Production and Purification of Recombinant Collagen XVIII Polypeptides. *Col18a1* cDNAs encoding the entire N-terminal NC domain of long collagen XVIII with (DUF-Fz-Tsp1) and without the Tsp1 region (DUF-Fz), plus the DUF domain alone, were adjoined to a C-terminal histidine tag and cloned into pcDNA3.1(+) (Invitrogen). Primers are described in Table S7. The constructs were transfected with FuGENE 6 Transfection Reagent (Roche) into HEK293 cells and stable cell lines generated. Recombinant proteins were purified from the cell media by metal ion affinity chromatography (ProBond Purification System; Invitrogen), and dialyzed against 1× PBS, pH 7.0. When indicated, purified DUF-Fz-Tsp1 (7.5 μg) was digested with 0.33 mU heparitinase I/μg of protein units (Seikagaku) at 37 °C for 2 h.

***Wnt10b* Coimmunoprecipitation.** Murine *Wnt10b* cDNA was inserted into pcDNA3.1/V5-HIS (Invitrogen) and transfected into specified HEK293 cell lines. Primers are described in Table S7. Cells were harvested in native lysis buffer (Cell Signaling Technology), and incubated with the anti-medium/long antibody bound to sheep anti-rabbit magnetic beads (Dynal) in PBS, pH 7.4. Washing was performed with PBS, pH7.4, containing 1% Triton X-100 and 0.1% SDS. Immunoprecipitates were eluted in 4× sample buffer and Western blot analysis performed with an anti-V5 antibody (Invitrogen).

Analyses of Liver Sections. For Oil-red O staining (0.3%), samples were snap-frozen and embedded in Tissue-Tek OCT Compound (Sakura Finetechnical). Cryosections were fixed in 10% (wt/vol) neutral-buffered formalin. Nuclei were stained with hematoxylin. For immunoelectron microscopy, liver pieces were fixed in 4% (wt/vol) paraformaldehyde in 0.1 M phosphate buffer, pH 7.4, containing 2.5% (wt/vol) sucrose for 2 h and then immersed in 2.3 M sucrose. Cryosections (60–70 nm) were incubated in 0.05 mM glycine in PBS, followed by incubation in 5% (wt/vol) BSA and 0.1% gelatin (Aurion) in PBS and exposed to the anti–medium/long-18 antibody and protein A-gold (10 nm) conjugates, both diluted in PBS containing 0.1% BSA-C. Controls were incubated with no primary antibody. Cryosections were embedded in methylcellulose and examined with a Tecnai Spirit microscope.

ApoE Binding Studies. Anti–medium/long-18 antibodies were bound to sheep anti-rabbit beads (Dynal) and incubated with 80 μL liver homogenate (1 g tissue per milliliter PBS). Captured proteins were resuspended in 20 μL of 4× sample buffer and size-fractionated in 6% (wt/vol) SDS/PAGE and Western blotted with an anti-mouse apoE antibody (Santa Cruz Biotechnology). In a solid-phase binding assay, ApoE3 (Invitrogen; 5 μg/mL in 100 μL PBS, pH7.4, per well) was immobilized in 96-well microtiter plates (Maxisorp; Nalgene Nunc) by an overnight 4 °C incubation. Wells were washed twice with 1× PBS, pH 7.4, 0.05% Tween 20 (PBST). Blocking was performed with 5% (wt/vol) nonfat milk for 1.5 h at room temperature. Specified amounts of purified DUF-Fz-Tsp1 and heparitinase-treated DUF-Fz-Tsp1 (diluted in PBS) were added to wells and incubated for 2.5 h at 37 °C. Incubations with the anti–medium/long-18 [1 μg/mL in 5% (wt/vol) nonfat milk] and secondary [HRP-conjugated goat anti-rabbit IgG, 1:5,000 in 5% (wt/vol) nonfat milk] antibodies were each for 1 h at room temperature. The 3,3′,5,5′-tetramethylbenzidine substrate reaction was terminated after 13 min with 0.2 M H_2SO_4. Absorbance was measured with a plate reader (Victor; PerkinElmer).

Lipid, Lipoprotein, and Activity Assays. Blood samples were collected by cardiac puncture after fasting for >3 h. Serum total cholesterol, free cholesterol, phospholipids, and triglycerides were measured by enzymatic colorimetry (53). Esterified cholesterol was calculated as total cholesterol minus free cholesterol. HDL-C was estimated after heparin-$MnCl_2$ precipitation of apoB-containing lipoproteins (53). FPLC-lipoprotein profiles were analyzed from pooled serum samples after gel-filtration separation of 100 μL of serum on a superose-6 column (Amersham Biosciences) in PBS-0.5 mM EDTA. For cholesterol and triglyceride determinations, 0.5-mL fractions were collected and concentrated to dryness. Heparin (0.1 U/g; Sigma) was injected into tail veins of 2-mo-old mice, and blood samples collected by cardiac puncture after 15 min. LPL, HL, and PLTP assays were performed as previously described (54, 55).

Statistical Analysis. Results are presented as mean ± SD. Differences between two groups (each mutant line compared with WT) were tested for statistical significance with a two-tailed Student *t* test. *P* values less than 0.05 were considered significant. $*P < 0.05$, $**P < 0.01$, $***P < 0.001$.

ACKNOWLEDGMENTS. We thank surgeons P. Käkelä and S. Venesmaa for fat biopsy collection, J. Peters and P. Tuomaala for technical assistance, L. Guasti and A. Dean for reading of the manuscript, and the Biocenter Oulu transgenic and electron microscopy facilities and Marshfield Mammalian Genotyping

Centre (WI) for their services. This study was funded in part by the Health Science Council of the Academy of Finland (Grant 138866 and Centre of Excellence 2012-2017 Grant 251314), the Sigrid Jusélius and the Diabetes Research Foundations, and the British Heart Foundation and Medical Research Council.

1. Hynes RO (2012) The evolution of metazoan extracellular matrix. *J Cell Biol* 196(6): 671–679.
2. Dong S, Cole GJ, Halfter W (2003) Expression of collagen XVIII and localization of its glycosaminoglycan attachment sites. *J Biol Chem* 278(3):1700–1707.
3. O'Reilly MS, et al. (1997) Endostatin: An endogenous inhibitor of angiogenesis and tumor growth. *Cell* 88(2):277–285.
4. Sertié AL, et al. (2000) Collagen XVIII, containing an endogenous inhibitor of angiogenesis and tumor growth, plays a critical role in the maintenance of retinal structure and in neural tube closure (Knobloch syndrome). *Hum Mol Genet* 9(13):2051–2058.
5. Khan AO, Aldahmesh MA, Mohamed JY, Al-Mesfer S, Alkuraya FS (2012) The distinct ophthalmic phenotype of Knobloch syndrome in children. *Br J Ophthalmol* 96(6): 890–895.
6. Kliemann SE, Waetge RT, Suzuki OT, Passos-Bueno MR, Rosemberg S (2003) Evidence of neuronal migration disorders in Knobloch syndrome: Clinical and molecular analysis of two novel families. *Am J Med Genet A* 119A(1):15–19.
7. Mahajan VB, et al. (2010) Collagen XVIII mutation in Knobloch syndrome with acute lymphoblastic leukemia. *Am J Med Genet A* 152A(11):2875–2879.
8. Fukai N, et al. (2002) Lack of collagen XVIII/endostatin results in eye abnormalities. *EMBO J* 21(7):1535–1544.
9. Ylikärppä R, et al. (2003) Lack of type XVIII collagen results in anterior ocular defects. *FASEB J* 17(15):2257–2259.
10. Utriainen A, et al. (2004) Structurally altered basement membranes and hydrocephalus in a type XVIII collagen deficient mouse line. *Hum Mol Genet* 13(18):2089–2099.
11. Bishop JR, et al. (2010) Deletion of the basement membrane heparan sulfate proteoglycan type XVIII collagen causes hypertriglyceridemia in mice and humans. *PLoS ONE* 5(11):e13919.
12. Moulton KS, et al. (2004) Loss of collagen XVIII enhances neovascularization and vascular permeability in atherosclerosis. *Circulation* 110(10):1330–1336.
13. Muragaki Y, et al. (1995) Mouse Col18a1 is expressed in a tissue-specific manner as three alternative variants and is localized in basement membrane zones. *Proc Natl Acad Sci USA* 92(19):8763–8767.
14. Rehn M, Pihlajaniemi T (1995) Identification of three N-terminal ends of type XVIII collagen chains and tissue-specific differences in the expression of the corresponding transcripts. The longest form contains a novel motif homologous to rat and Drosophila frizzled proteins. *J Biol Chem* 270(9):4705–4711.
15. Saarela J, Rehn M, Oikarinen A, Autio-Harmainen H, Pihlajaniemi T (1998) The short and long forms of type XVIII collagen show clear tissue specificities in their expression and location in basement membrane zones in humans. *Am J Pathol* 153(2):611–626.
16. Rehn M, Hintikka E, Pihlajaniemi T (1996) Characterization of the mouse gene for the alpha 1 chain of type XVIII collagen (Col18a1) reveals that the three variant N-terminal polypeptide forms are transcribed from two widely separated promoters. *Genomics* 32(3):436–446.
17. Elamaa H, Snellman A, Rehn M, Autio-Harmainen H, Pihlajaniemi T (2003) Characterization of the human type XVIII collagen gene and proteolytic processing and tissue location of the variant containing a frizzled motif. *Matrix Biol* 22(5):427–442.
18. Quélard D, et al. (2008) A cryptic frizzled module in cell surface collagen 18 inhibits Wnt/beta-catenin signaling. *PLoS ONE* 3(4):e1878.
19. Kinnunen AI, et al. (2011) Lack of collagen XVIII long isoforms affects kidney podocytes, whereas the short form is needed in the proximal tubular basement membrane. *J Biol Chem* 286(10):7755–7764.
20. Boudko SP, et al. (2009) Crystal structure of human collagen XVIII trimerization domain: A novel collagen trimerization Fold. *J Mol Biol* 392(3):787–802.
21. Rodeheffer MS, Birsoy K, Friedman JM (2008) Identification of white adipocyte progenitor cells in vivo. *Cell* 135(2):240–249.
22. Hausman GJ, Hausman DB (2006) Search for the preadipocyte progenitor cell. *J Clin Invest* 116(12):3103–3106.
23. Smink JJ, Leutz A (2012) Instruction of mesenchymal cell fate by the transcription factor C/EBPβ. *Gene* 497(1):10–17.
24. Park BO, Ahrends R, Teruel MN (2012) Consecutive positive feedback loops create a bistable switch that controls preadipocyte-to-adipocyte conversion. *Cell Reports* 2(4):976–990.
25. Gustafson B, Smith U (2010) Activation of canonical wingless-type MMTV integration site family (Wnt) signaling in mature adipocytes increases beta-catenin levels and leads to cell dedifferentiation and insulin resistance. *J Biol Chem* 285(18): 14031–14041.
26. John E, et al. (2012) Dataset integration identifies transcriptional regulation of microRNA genes by PPARγ in differentiating mouse 3T3-L1 adipocytes. *Nucleic Acids Res* 40(10):4446–4460.
27. Shen L, Glowacki J, Zhou S (2011) Inhibition of adipocytogenesis by canonical WNT signaling in human mesenchymal stem cells. *Exp Cell Res* 317(13):1796–1803.
28. Wright WS, et al. (2007) Wnt10b inhibits obesity in ob/ob and agouti mice. *Diabetes* 56(2):295–303.
29. Lefterova MI, et al. (2008) PPARgamma and C/EBP factors orchestrate adipocyte biology via adjacent binding on a genome-wide scale. *Genes Dev* 22(21):2941–2952.
30. Thompson GM, et al. (2004) A high-capacity assay for PPARgamma ligand regulation of endogenous aP2 expression in 3T3-L1 cells. *Anal Biochem* 330(1):21–28.
31. Hendaoui I, et al. (2012) Inhibition of Wnt/β-catenin signaling by a soluble collagen-derived frizzled domain interacting with Wnt3a and the receptors frizzled 1 and 8. *PLoS ONE* 7(1):e30601.
32. Kaminska D, et al. (2012) Adipose tissue TCF7L2 splicing is regulated by weight loss and associates with glucose and fatty acid metabolism. *Diabetes* 61(11):2807–2813.
33. Lee SJ, Grosskopf I, Choi SY, Cooper AD (2004) Chylomicron remnant uptake in the livers of mice expressing human apolipoproteins E3, E2 (Arg158→Cys), and E3-Leiden. *J Lipid Res* 45(12):2199–2210.
34. Raffaï RL, et al. (2003) Hepatocyte-derived ApoE is more effective than non-hepatocyte-derived ApoE in remnant lipoprotein clearance. *J Biol Chem* 278(13): 11670–11675.
35. González-Navarro H, et al. (2004) The ligand-binding function of hepatic lipase modulates the development of atherosclerosis in transgenic mice. *J Biol Chem* 279(44):45312–45321.
36. Ji ZS, Dichek HL, Miranda RD, Mahley RW (1997) Heparan sulfate proteoglycans participate in hepatic lipaseand apolipoprotein E-mediated binding and uptake of plasma lipoproteins, including high density lipoproteins. *J Biol Chem* 272(50): 31285–31292.
37. Lee SJ, et al. (2005) Removal of chylomicron remnants in transgenic mice overexpressing normal and membrane-anchored hepatic lipase. *J Lipid Res* 46(1):27–35.
38. Luo Y, et al. (2010) Pharmacologic inhibition of phospholipid transfer protein activity reduces apolipoprotein-B secretion from hepatocytes. *J Pharmacol Exp Ther* 332(3): 1100–1106.
39. Yazdanyar A, Jiang XC (2012) Liver phospholipid transfer protein (PLTP) expression with a PLTP-null background promotes very low-density lipoprotein production in mice. *Hepatology* 56(2):576–584.
40. Rosen ED, Spiegelman BM (2014) What we talk about when we talk about fat. *Cell* 156(1–2):20–44.
41. Cawthorn WP, et al. (2012) Wnt6, Wnt10a and Wnt10b inhibit adipogenesis and stimulate osteoblastogenesis through a β-catenin-dependent mechanism. *Bone* 50(2): 477–489.
42. Kennell JA, MacDougald OA (2005) Wnt signaling inhibits adipogenesis through beta-catenin-dependent and -independent mechanisms. *J Biol Chem* 280(25):24004–24010.
43. Ross SE, et al. (2000) Inhibition of adipogenesis by Wnt signaling. *Science* 289(5481): 950–953.
44. Udagawa N, et al. (1989) The bone marrow-derived stromal cell lines MC3T3-G2/PA6 and ST2 support osteoclast-like cell differentiation in cocultures with mouse spleen cells. *Endocrinology* 125(4):1805–1813.
45. Longo KA, et al. (2004) Wnt10b inhibits development of white and brown adipose tissues. *J Biol Chem* 279(34):35503–35509.
46. So JS, et al. (2012) Silencing of lipid metabolism genes through IRE1α-mediated mRNA decay lowers plasma lipids in mice. *Cell Metab* 16(4):487–499.
47. Peloso GM, et al.; NHLBI GO Exome Sequencing Project (2014) Association of low-frequency and rare coding-sequence variants with blood lipids and coronary heart disease in 56,000 whites and blacks. *Am J Hum Genet* 94(2):223–232.
48. North KE, et al. (2005) Evidence for a gene influencing fasting LDL cholesterol and triglyceride levels on chromosome 21q. *Atherosclerosis* 179(1):119–125.
49. Hannukainen JC, et al. (2010) Higher free fatty acid uptake in visceral than in abdominal subcutaneous fat tissue in men. *Obesity (Silver Spring)* 18(2):261–265.
50. Aikio M, et al. (2013) Collagen XVIII short isoform is critical for retinal vascularization, and overexpression of the Tsp-1 domain affects eye growth and cataract formation. *Invest Ophthalmol Vis Sci* 54(12):7450–7462.
51. Livak KJ, Schmittgen TD (2001) Analysis of relative gene expression data using real-time quantitative PCR and the 2(-Delta Delta C(T)) Method. *Methods* 25(4):402–408.
52. Joe AW, Yi L, Even Y, Vogl AW, Rossi FM (2009) Depot-specific differences in adipogenic progenitor abundance and proliferative response to high-fat diet. *Stem Cells* 27(10):2563–2570.
53. Mäkelä SM, et al. (2008) HDL2 of heavy alcohol drinkers enhances cholesterol efflux from raw macrophages via phospholipid-rich HDL 2b particles. *Alcohol Clin Exp Res* 32(6):991–1000.
54. Ehnholm C, Kuusi T (1986) Preparation, characterization, and measurement of hepatic lipase. *Methods Enzymol* 129:716–738.
55. Jauhiainen M, Ehnholm C (2005) Determination of human plasma phospholipid transfer protein mass and activity. *Methods* 36(2):97–101.